# Direct magnetic resonance detection of neuronal electrical activity

**Natalia Petridou*, Dietmar Plenz†, Afonso C. Silva‡, Murray Loew§, Jerzy Bodurka¶, and Peter A. Bandettini*¶‖**

*Section on Functional Imaging Methods, Laboratory of Brain and Cognition, †Neural Network Physiology Unit, Laboratory of Systems Neuroscience, and ¶Functional MRI Facility, National Institute of Mental Health, National Institutes of Health, Bethesda, MD 20892; ‡Cerebral Microcirculation Unit, Laboratory of Functional and Molecular Imaging, National Institute of Neurological Disorders and Stroke, National Institutes of Health, Bethesda, MD 20892; and §Institute for Medical Imaging and Image Analysis, Department of Electrical and Computer Engineering, George Washington University, Washington, DC 20052

Edited by Marcus E. Raichle, Washington University School of Medicine, St. Louis, MO, and approved September 5, 2006 (received for review April 20, 2006)

**Present noninvasive neuroimaging methods measure neuronal activity indirectly, via either cerebrovascular changes or extracranial measurements of electrical/magnetic signals. Recent studies have shown evidence that MRI may be used to directly and noninvasively map electrical activity associated with human brain activation, but results are inconclusive. Here, we show that MRI can detect cortical electrical activity directly. We use organotypic rat-brain cultures *in vitro* that are spontaneously active in the absence of a cerebrovascular system. Single-voxel magnetic resonance (MR) measurements obtained at 7 T were highly correlated with multisite extracellular local field potential recordings of the same cultures before and after blockade of neuronal activity with tetrodotoxin. Similarly, for MR images obtained at 3 T, the MR signal changed solely in voxels containing the culture, thus allowing the spatial localization of the active neuronal tissue.**

cell culture | functional MRI | neuronal current imaging | brain

Present noninvasive neuroimaging methods have provided a wealth of information regarding the dynamic spatial and temporal organization of the brain. Limitations nevertheless remain. Electroencephalography (EEG) and magnetoencephalography (MEG) measure electromagnetic neuronal activity on the surface of the scalp with millisecond temporal resolution but limited spatial resolution and certainty of activation location (1–4). Functional MRI (fMRI) methods measure localized changes of blood flow, blood volume, and/or blood oxygenation that occur with increased neuronal activation. The spatial (1.5–3 mm) and temporal resolution (1 s) of functional MRI is limited by variations in the vasculature and the neuronal-hemodynamic coupling (5). Significant effort has been made, with limited success, to combine information from these different methods to obtain more accurate maps of brain activation (4, 6).

The work presented here presents evidence that magnetic resonance (MR) can detect changes in magnetic field, not related to hemodynamic changes but induced by neuronal electrical activity. The MR signal originates from protons precessing at a given frequency that is proportional to the magnetic field that they are experiencing. Ionic currents, on the order of a few nanoamperes, that are associated with synaptic and suprathreshold activity result in weak magnetic fields. These fields alter the precession frequency of the surrounding protons and, therefore, may create a small change in the measured MR phase and/or MR magnitude signal. Magnitude changes are caused by a destructive addition of multiple different frequency offsets within a voxel. Phase changes are measurable if a substantial proportion of protons in a voxel have the same frequency offset.

MR imaging of weak magnetic field changes has been demonstrated in phantoms (7–11), in snail ganglia (12, 13), and in the human body by using experimentally applied current (14). Although not conclusive, reports of using MRI to detect neuronal activity-based signal changes in the human brain have been published (15–19). A primary assumption involving the separation of neuronal from hemodynamic signals is that fast signal changes are uniquely indicative of rapidly occurring neuronal electrical activity, whereas slow signal changes are uniquely associated with hemodynamic processes. Fast signal changes, however, cannot be decisively separated from hemodynamic effects because the hemodynamic signal also may show small fluctuations at a fast time scale (<200 ms) (19). The main challenges remain to convincingly demonstrate that magnetic fields originating from intrinsic cortical currents can be detected with MRI and to clearly separate the ubiquitous hemodynamic effects on the MR signal from the hypothesized direct neuronal-electric effects.

In this study, we adopted an approach that avoided the potentially confounding effects of hemodynamic changes associated with neuronal activity. We used organotypic rat-brain cultures *in vitro* that display bursts of spontaneous neuronal activity in the absence of a cerebrovascular system (20). We made use of the fact that bursts of activity are reflected by a high signal power at a culture-specific frequency range. We manipulated the state of activity pharmacologically by means of tetrodotoxin (TTX), which blocks sodium channels. MR measurements were obtained during spontaneous neuronal activity, followed by measurements of activity blocked with TTX infusion. Evidence for MR detection of neuronal electrical activity would be provided if the MR signal power was reduced after TTX infusion. Because electrical activity theoretically can produce both phase and magnitude changes, both phase and magnitude MR data were examined.

Two sets of experiments, (*i*) to assess the sensitivity of MR-based detection of neuronal electrical activity and (*ii*) to assess the potential for conventional imaging applications to localize these changes, were performed. In the first experiment, imaging was not performed. Rather, MR measurements were obtained by using a 7-T MR scanner and a free induction decay (FID) technique that allows high temporal resolution and sensitivity. The cultures were grown on 60-channel multielectrode arrays (MEA) that allowed for multisite local field potential (LFP) recordings (21) before and after the MR sessions. These recordings were compared with MR measurements obtained from each culture. Correlation between signal power changes at the culture activation frequency range, obtained with both techniques, would be clear evidence that neuronal activity is directly detectable by MR. The second experiment was performed by using a 3-T MR scanner with a conventional imaging technique and no electrical recordings.

Author contributions: N.P., D.P., A.C.S., M.L., J.B., and P.A.B. designed research; N.P., D.P., A.C.S., and J.B. performed research; N.P., J.B., and P.A.B. analyzed data; and N.P., J.B., and P.A.B. wrote the paper.

The authors declare no conflict of interest.

This article is a PNAS direct submission.

Abbreviations: EEG, electroencephalography; FID, free induction decay; LFP, local field potential; MEA, multielectrode array; MEG, magnetoencephalography; MR, magnetic resonance; PRE, preceding administration of TTX; SE EPI, spin-echo echo planar imaging; TTX, tetrodotoxin.

‖To whom correspondence should be addressed. E-mail: bandettini@nih.gov.

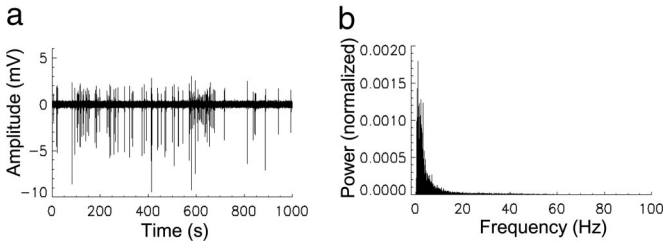


**Fig. 1.** EEG showing the spontaneous synchronized neuronal activity in one culture. (*a*) Net activity exhibited in the culture over a period of 1,000 s (≈17 min) obtained from averaging the 60 MEA channels. (*b*) Power spectrum of the EEG shown in *a*. High power associated with activity is concentrated in the <15 Hz range. The power spectrum range is 0–500 Hz (sampling at 1 kHz); however, for visibility, only 0–100 Hz is shown.

## Results

**Detection of Neuronal Electrical Activity.** After 3–4 weeks of development, the organotypic tissue cultures covered an area of ≈4 × 8 mm on the MEA reaching a thickness of ≈60–100 $\mu$m that is equivalent to ≈20,000–70,000 neurons. The cultures exhibited spontaneous activity characterized by bursts of synchronized rhythmic activity that lasts for several seconds followed by several seconds of quiescence. Fast inhibition was blocked by bath application of the $GABA_A$ antagonist picrotoxin (10 $\mu$M) to increase spontaneous activity. During the resulting epileptic activity, spikes and synaptic inputs were synchronized with millisecond precision, which resulted in large LFP signals that lasted for 100–200 ms and were recorded with the MEA. The LFP activity in this preparation showed prominent population spikes that are indicative of action potentials from many neurons being synchronized (20). LFP activity was blocked after TTX infusion (10 $\mu$M) (Fig. 5, which is published as supporting information on the PNAS web site). The bursts of activity occurred at a low frequency between ≈0.01 and ≈0.2 Hz and consisted of LFPs occurring with a frequency up to ≈15 Hz for the duration of the burst (Fig. 1).

Time series of the MR signal FID were obtained from seven cultures at 7 T during spontaneous neuronal activity [preceding administration of TTX (PRE) state, ≈17 min], and during the ensuing inactive state after TTX infusion (TTX state, ≈17 min). MR signals were acquired every 100 ms, which matched the duration of a single LFP, and were obtained from a single volume (40 $mm^3$) that encompassed the culture. EEG measurements were obtained immediately before and after each MR session, which corresponded to the PRE and TTX states for the given culture. For two of the seven cultures, EEG measurements were obtained for an additional period of 60 min before the MR measurements to examine the temporal stability of activation. A control experiment also was performed in identical conditions as described above but without neuronal tissue on the MEA. The control measurements were used to help identify any MR signal components not related to neuronal activity. Because of a technical problem, the EEG measurements obtained from two cultures were discarded. Power spectra were obtained from the five remaining EEG and all MR time series for the PRE and TTX states. The spectra were compared between the two states to identify decreases in signal power that indicated the suppression of neuronal activity after TTX infusion. For three of the seven cultures, control EEG measurements were obtained after the replacement of the TTX-infused culture medium with standard medium as to reinstate neuronal activity (wash state). The EEG wash spectra were compared with the corresponding EEG TTX spectra to confirm that signal power decreases in the TTX state were due to the suppression of activity in the cultures. The MR spectra were compared with the corresponding EEG spectra to investigate whether power decreases observed in the MR spectra corresponded in the frequency range

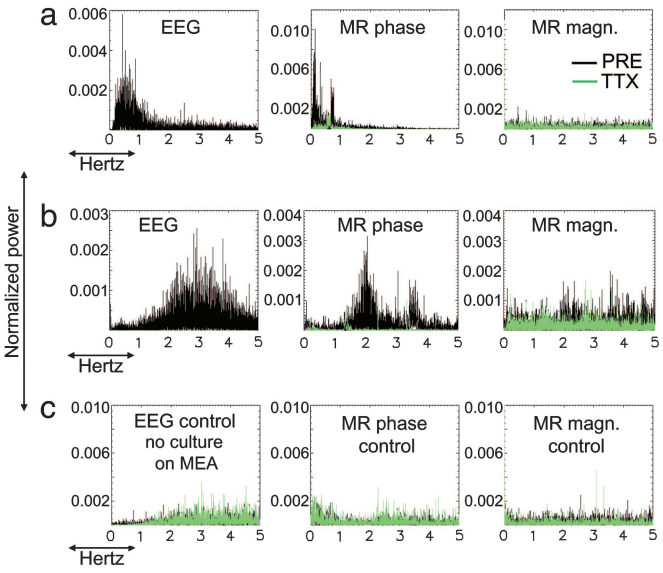


**Fig. 2.** EEG and MR spectra obtained from two cultures (*a* and *b*) plus the control (*c*). To compare between the MR and EEG spectra, only the 0–5 Hz frequency range is shown for the EEG. (*a* and *b*) Signal power is reduced after TTX administration (green vs. black lines). Residual peaks in the TTX phase spectra, also present in the PRE state, are possibly due to systematic noise. (*c*) For the control experiment, there was no significant change in signal power after TTX administration.

of the culture's activity. The amplitude-weighted spectral mean frequency was used to evaluate the distribution of frequencies in each spectrum.

The five EEG data sets showed a decrease in signal power in the TTX state as compared with the PRE state (power decrease: 83.6 ± 19.4%). The corresponding MR data sets also showed a decrease in the signal power in the TTX state as compared with the PRE state; however, the effect was more pronounced for MR phase than for MR magnitude (power decrease 57.6 ± 24.5% and 12.4 ± 10.2%, respectively) (Figs. 2 and 3*a*). The three EEG wash data sets showed the recovery of spontaneous neuronal activity in the cultures (wash signal power increase: 94.6 ± 2.5%) (Fig. 6, which is published as supporting information on the PNAS web site). When including all seven cultures for the MR data analysis, similar results were obtained (PRE vs. TTX signal power decrease for MR phase 60.5 ± 21.5% and for MR magnitude 18.8 ± 16.3%). Linear regression on the EEG and the corresponding MR phase data ($n$ = 5) for the PRE vs. TTX signal power decrease yielded a close

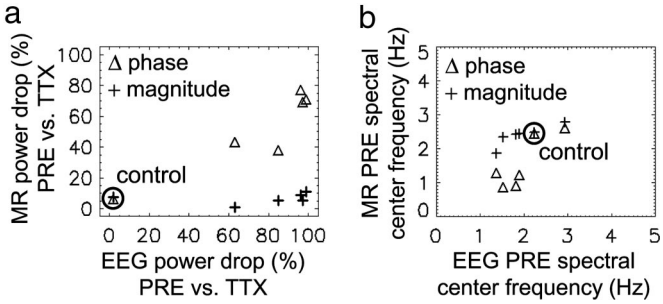


**Fig. 3.** Comparison between EEG and MR data. (*a*) Signal power decrease (0–5 Hz) between PRE and TTX states, for MR magnitude (+), and MR phase (Δ) vs. EEG ($n$ = 5, plus control). (*b*) Spectral center frequency (spectral centroid 0–5 Hz) for MR magnitude (+) and MR phase (Δ) vs. EEG ($n$ = 5, plus control). The control experiment was performed with no culture on the MEA, but all other conditions were identical.

correspondence between the two measurements ($R^2 = 0.83$, $P = 0.01$; Fig. 3*a*). Linear regression on the EEG and MR magnitude data for the PRE vs. TTX signal power decrease did not reveal a significant correspondence between the two measurements ($R^2 = 0.04$, $P = 0.12$; Fig. 3*a*).

MR spectral peaks that showed decreased power in the TTX state were within the frequency range of the individual culture's activity as measured from the EEG spectra (Figs. 2 and 3*b*) (PRE state spectral mean frequency 1.55 ± 0.77 Hz for MR phase and 1.96 ± 0.57 Hz for EEG; TTX state spectral mean frequency 1.87 ± 0.15 Hz for MR phase and 2.26 ± 0.28 Hz for EEG). Linear regression on the EEG and MR phase spectral mean frequency for the PRE state yielded a close correspondence between the two measurements ($R^2 = 0.80$, $P = 0.015$; Fig. 3*b*). Correlation between the EEG and MR phase spectra also revealed a correspondence between the two measurements even though differences in spectral characteristics were observed (Fig. 2) [correlation ($\rho$) = 0.4 ± 0.1, $P < 10^{-4}$ between EEG and MR phase spectra for the PRE state; $\rho = -0.007 \pm 0.11$, $10^{-4} < P < 0.2$ for the TTX state]. However, similar differences in spectral characteristics were observed between the EEG spectra obtained for different time periods for the initial two cultures ($\rho = 0.25 \pm 0.03$, $P \approx 0$ between EEG spectra for a ≈45-min time difference between recordings and $\rho = 0.42 \pm 0.05$, $P \approx 0$ for consecutive time periods).

For the control experiment, a signal power decrease also was observed between the PRE and TTX states for the entire spectral range (0–5 Hz) but at a much lower level of 6.4% for MR phase and 7.4% for MR magnitude (vs. 2.17% for EEG) (Figs. 2*c* and 3*a*). The distribution of frequencies for the control data for both EEG and MR was equivalent to random noise (spectral mean frequency ≈2.5 Hz for both states).

The signal changes observed ($n = 7$) ranged from ≈0.15 to ≈3° for MR phase and 0.01 (below noise level) to 0.4% for MR magnitude. The corresponding magnetic field changes were on the order of ≈0.2 to ≈3.9 nT.

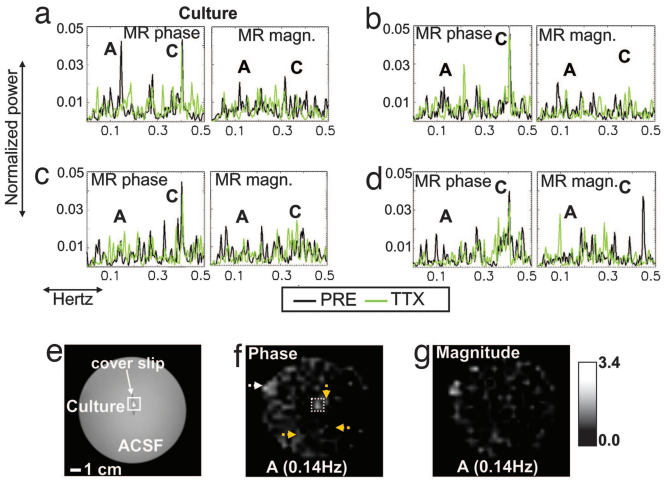


**Fig. 4.** Imaging results obtained for one culture. (*a*) Single-voxel phase and magnitude spectra for the culture region. (*b–d*) Single-voxel phase and magnitude spectra for three artificial cerebrospinal fluid (ACSF) locations. A peak corresponding to the culture site is observed solely in the PRE phase spectrum, marked as A (≈0.14 Hz), possibly representing the activation burst frequency of the culture. The spectral peak marked as C corresponds to the scanner cooling-pump frequency and is present in all conditions. (*e*) Structural fast-spin-echo image obtained during the same MR session. (*f* and *g*) Phase map (*f*) and magnitude map (*g*), showing the difference in signal power between the PRE and TTX conditions for peak A. The spectra shown in *a* correspond to a voxel in the culture area indicated by the box in *e* and *f*. The spectra shown in (*b–d*) are marked by orange arrows on the phase map (clockwise from culture). The increased signal power for peak A is localized on the culture in the phase map, seen also in the overplot of A on the anatomical image in *e*. The high-intensity region indicated by the white arrow (*f*, upper left) reflects elevated signal power in the PRE state at all frequencies, possibly due to hardware instabilities or imperfect shimming.

**Detection and Mapping of Neuronal Electrical Activity.** To assess the potential of conventional imaging methods to detect and map this effect, four cultures were scanned at 3 T by using a single-shot spin-echo echo-planar (SE EPI) MR image acquisition (8). Because of image distortion in the culture medium vs. air interface in the MEA chamber, epileptic cultures were prepared on glass coverslips and immersed in a spherical container filled with artificial cerebrospinal fluid (no picrotoxin added). MR images were acquired for the PRE, followed by the TTX, states for a total of 10 min per state. An image was acquired every second, which is within the range used for functional MRI applications. At the temporal resolution of 1 s, neuronal activity was undersampled, therefore we expected to capture only the bursts of activity, occurring in the ≈0.01 to ≈0.2 Hz range, and we anticipated reduced signal changes as compared with the 7-T measurements. Similar to the 7-T experiment, detection of neuronal activation signals was assessed by a reduction in signal power between the PRE and TTX states.

Power spectra were obtained from the MR time series on a voxelwise basis. The spectra were compared between the PRE and TTX states per voxel to investigate whether power decreases in the MR spectra were observed in the voxels corresponding to the culture location. In three of four cultures, the comparison revealed a reduction in signal power selectively in voxels that contained the culture (mean signal power reduction 36 ± 18% for voxels corresponding to the culture location and 9.3 ± 7% for voxels corresponding to artificial cerebrospinal fluid; Fig. 4 *a–d*). The effect was observed in the phase data but not in the magnitude data. The signal power decrease was observed in the 0.1–0.2 Hz range of the phase power spectrum (Fig. 4*a*). Maps of the signal power decrease for the phase spectral peaks in that range exhibited the maximum value localized on the culture (Fig. 4 *e* and *f*; see also Fig. 7, which is published as supporting information on the PNAS web site). The phase changes observed ($n = 3$) were on the order of ≈0.2–0.8°, translating to ≈0.2 to ≈1 nT.

## Discussion

In two MR experiments, we found time series MR signal changes that relate to neuronal electrical activity. The results cannot be attributed to hemodynamic phenomena because the cultures were devoid of blood cells and a vascular system. The first experiment, performed at 7 T with a single voxel, revealed MR signal spectral power increases within the frequency range of activity bursts as measured with EEG in the same cultures. Furthermore, the spectral power at those frequencies disappeared after blocking neuronal activity with TTX in both the EEG and the MR signals. In the imaging experiment performed at 3 T, we confirmed that the changes in MR signal were specific for the cultures because the changes occurred only in voxels containing tissue.

For the 7-T experiment, where the MR data acquisition rate was matched to the LFP duration, we observed changes in the MR signal equivalent to those observed in the EEG recordings. Each culture exhibited a unique activation pattern, which resulted in a unique EEG spectral pattern and signal power decrease after the suppression of activity with TTX. A similar spectral pattern and signal power decrease was observed in the MR phase for the corresponding culture (Figs. 2 and 3). This pattern similarity suggests that MR may be sensitive to different levels of activity in the cortex. However, MR spectral peaks consistently appeared at lower frequencies as compared with the EEG spectral peaks, and differences in spectral characteristics were observed (Figs. 2 and 3*b*). This observation may be due to the fact that the recordings were not performed concurrently, there were different sources of noise, and, perhaps, there was different sensitivity to neuronal signal changes. If LFPs of small magnitude were undetected by MR,

then the MR spectra would have different spectral content and a narrower distribution than the EEG spectra due to the properties of the Fourier transform (22). Similarly, if the LFP duration did not exactly coincide with the duration of the MR signal acquisition but spanned more than one signal acquisition, then the MR spectral peaks would appear at lower frequencies as compared with the EEG spectra. Differences in spectral characteristics also were observed between the EEG spectra obtained at different time points for two cultures, which suggests that some spectral variability may be due to time-dependent changes in the activity of the cultures. A linear relationship, however, was observed between MR phase and EEG with respect to signal power decrease after TTX infusion and spectral mean frequencies (Fig. 3). A signal power decrease also was observed between the PRE and TTX states for the control experiment but at a much lower level. Such power decrease may be related to changes in the culture medium composition because of the TTX infusion.

For the 3-T imaging experiment where the MR acquisition was slower (1 s), the MRI signal changes detected were within the frequency range of activity bursts for the cultures used (≈0.01 to ≈0.2 Hz). A signal power decrease after TTX infusion for peaks in that range was observed solely in the voxels containing the culture (≤3), suggesting that the signal power reduction originated from the suppression of neuronal activity in the culture (Fig. 4). The effect was observed only in the MR phase data.

In summary, the decrease in signal power with TTX for both the 7-T and 3-T experiments, but also the correspondence of EEG and 7-T MR spectra in frequencies up to 5 Hz, suggests that the observed MR signal changes are most likely due to synchronized electric activity across neurons. According to MEG measurements, evoked or spontaneous synchronized synaptic activity in 50,000 or more cortical neurons that occupy an area of one or a few $mm^2$ results in magnetic fields on the order of $10^{-13}$ to $10^{-12}$ T at a distance of 2–4 cm away from the neuronal source (2, 4). Assuming a ≈2- to 4-mm measurement range of an MR voxel encompassing the site of activation, those fields are on the order of $10^{-10}$ to $10^{-9}$ T [distance scale $(r_{MEG}/r_{MR})^2$; ref. 8], equivalent to those observed from our *in vitro* cultures (≈0.2–3.9 nT).

**The MR Signal Change.** The signal changes observed in MR magnitude were less pronounced than MR phase, which may be expected if the synchronized LFP activity observed in the cultures resulted in a homogeneous magnetic field. The MR signal arises from proton precession at a given frequency depending on the magnetic field they experience and decays primarily due to variations in the precession frequency due to local magnetic fields in the sample. Neuronal magnetic fields could induce either a bulk modulation in the proton precession frequency, or phase shift, or increased variations in the precession frequency, or phase dispersion, or both. If the neuronal magnetic field is mainly homogeneous inside a voxel, a phase shift will occur. If it is mainly inhomogeneous, phase dispersion will occur. The homogeneity of the neuronal magnetic field inside a voxel depends, among other things, on the spatiotemporal coherence and the extent of activation with respect to the voxel volume. Recent theoretical modeling suggests that magnetic fields of individual neurons may result in an inhomogeneous magnetic field inside the voxel (23). Alternatively, MEG theory suggests that magnetic fields originating from synchronized postsynaptic activity in groups of pyramidal neurons parallel to each other, as was the case with our cultures, summate (1), which may result in a homogeneous field inside the voxel. Whereas phase dispersion translates to cancellation of phase signals, phase shift translates to larger signal changes for MR phase as compared with MR magnitude. For the 7-T experiment, significant MR magnitude changes were observed for three of seven cultures (Figs. 2*b* and 3*a*), possibly due to a higher level of activity in the culture or a higher signal to noise achieved for the given culture. MR magnitude changes were below detection range at 3 T, which may be due to the lower signal to noise achieved at 3 T as compared with 7 T. The above observations suggests that for this particular setup, the dominant source of MR contrast was coherence in signal and magnetic field shifts at a larger scale than individual neurons, resulting in larger phase shifts than magnitude changes.

**Other Potential Sources of the Signal.** Other potential sources of the signal change have been considered. It is possible that currents in the extracellular fluid (volume currents) associated with synaptic activity, as opposed to currents across synapses, contribute to the MR signal. However, recent studies on the feasibility of direct MR detection of neuronal electrical activity, as well as MEG studies, suggest that those currents are likely to have a negligible influence on the MR signal (11).

Another possibility is neuron motion due to Lorentz forces induced by the static magnetic field on firing neurons (9, 10). Provided that the neurons in our culture preparation are compliant, this neuron motion would induce a spatially incoherent displacement of the surrounding medium inside the voxel, which would result in phase dispersion and a magnitude change rather than the phase shifts observed in our data. It also should be noted that our MR measurements may have not been sensitive to Lorentz effects (9, 10).

We also considered that the MR signal changes could have originated from nonelectrical processes associated with neuronal activation. Temperature changes due to metabolic activity (24–26), motion of water molecules associated with ion flux across the cell membrane during activation, increased water content inside the neurons (cell swelling), or physical motion induced by the changes in cellular volume (27–30) all could be factors in the signal changes.

Metabolic activity can result in changes in local temperature on the order of one-tenth of a degree Celsius in a period of several seconds (24–26) These temperature changes may result in MR phase shifts of the same order as the ones observed. However, the phase changes observed in the 7-T data were considerably faster than what would be expected from secondary temperature changes and were not restricted to negative shifts as may be expected by a temperature increase due to metabolic activity. Considering that the voxel volume consisted primarily of culture medium maintained at a constant temperature, it is unlikely that the small local temperature changes can affect the overall signal from the whole volume.

Changes in ionic transmembrane flux during activation can cause changes in water diffusion in the extra/intracellular fluid (apparent diffusion coefficient changes) (27, 28). Changes in water diffusion, however, reflect the incoherent movement of water molecules, which results in random dephasing and cancellation of phase signals rather than a phase shift. This dephasing would result in a magnitude change. Nevertheless, we observed predominantly phase shifts and only minimal magnitude changes in our data.

The changes in ionic transmembrane flux and water diffusion also can result in increased water content inside the neuron (29, 30). The increased intracellular water content may induce a decrease in tissue magnetization decay time (T1) independent of current-induced effects and could be a source of the observed magnitude signal changes. Again, our observation of a predominant phase shift and minimal magnitude changes argues against this mechanism.

Finally, changes in cell volume can result in physical motion of the neurons (29). This motion however occurs in multiple directions, resulting in phase dispersion and a magnitude change rather than a phase shift.

In summary, several alternative explanations can be considered, but none can explain the results as completely as a change in an across-neurons magnetic field associated with neuronal activity.

This study demonstrates that MR phase and, to a lesser degree, magnitude changes associated with neuronal firing, can be detected in cell cultures devoid of blood. The compelling implication is that neuronal electrical activity can be measured and mapped directly

with MRI. The challenge that lies ahead is to achieve the same quality of results, and be able to separate them from hemodynamic changes, in humans for application in neuroscience.

Hemodynamic effects on MR signal are likely an order of magnitude larger than neuronal electric activity effects. Given the evidence provided in this paper that intrinsic cortical activity can be detected with MR, the main challenge is to separate the two effects cleanly.

## Materials and Methods

**Culture Preparation.** For the preparation of organotypic tissue cultures, somatosensory cortex and parts of the basal ganglia were taken from acute coronal slices of newborn rats (postnatal day 0–2). Organotypic cultures made from coronal slices maintain the layered organization of the cortex and the parallel orientation of pyramidal neurons with respect to each other (31). The tissue was cultured for up to 3–4 weeks on MEAs (Multi Channel Systems, Reutlingen, Germany) (20, 21). The MEA had an 8 × 8 electrode configuration (MR compatible gold electrodes, one reference, corner electrodes missing) covering an area of 1.8 $mm^2$, enclosed in an ≈20-mm diameter chamber (Fig. 8 *a* and *b*, which is published as supporting information on the PNAS web site). The acute slices were attached to the array by using a plasma-thrombin mixture and submerged in 800 $\mu$l of culture medium. A sealed culture chamber attached to the MEA allowed for sterile culture and recording conditions throughout the development inside an incubator at 35 ± 0.5°C. Medium was replaced every 3–4 days. This approach allowed for neuronal cultures to preserve most of the architectural specificity of a cortical and/or basal ganglia network.

**EEG Data Acquisition and Processing.** For extracellular LFP recordings, the culture attached to the MEA was placed under sterile conditions into a recording head stage inside the culture incubator (Multi Channel Systems). Recordings were performed before and after the MR sessions because the recording system contained magnetic and electronic components that could not be used inside the MR scanner. LFP activity was bandpass filtered between 1–60 Hz and continuously recorded at 1 kHz from all 60 electrodes for 20 min (electrode diameter, 30 $\mu$m; interelectrode distance, 200 $\mu$m; ref. 21). For the initial two cultures, measurements were obtained for an additional period of 60 min before the MR measurements. Recordings were performed in the presence of standard culture medium. For direct comparison between the EEG and MR recordings, the 60-channel LFP recordings were averaged in time, yielding a 1 million data-point average EEG (1 kHz sampling for 1,000 s; Fig. 1*a*). The resulting average EEG matched the spatial scale of the MR measurements. The EEG data sets were detrended to correct for linear drift.

**7-T NMR.** ***Experiment setup and data acquisition.*** The MEAs containing the cultures were secured on a custommade cradle, ≈20 cm in diameter, matching the bore size of the scanner. The temperature was held at 36 ± 0.5°C with an air temperature controller. MR data were acquired from seven cultures by using a 7-T Biospin MRI scanner (Bruker, Billerica, MA) (7 T/20 cm) with a custommade RF transmit/receive surface coil. Structural gradient-echo FLASH images were acquired for localization (image matrix, 128 × 128; slice thickness, 1 mm; field of view, 2 cm, one slice, coronal plane). Subsequently, a slice of 2 mm thickness was prescribed, which covered the entire neuronal culture, orthogonal to the reference electrode based on the localizer (Fig. 8*c*). The slice thickness was equal to the thickness of the reference electrode; the resulting voxel volume was 40 $mm^3$, restricted by the array chamber dimensions (20 mm) and culture medium level (≈1 mm). FID acquisition was used to obtain MR measurements from this voxel (repetition time, 100 ms; field of view, 2 cm; flip angle, 30°; readout window, 30–1 ms; dwell time, 40 $\mu$s, resulting in 1,024 data points per single FID; note that for the FID acquisition localizing magnetic fields, gradients are not applied). Each MR session involved two acquisitions: (*i*) PRE, neuronal activity present (10,100 FIDs, ≈17 min), and (*ii*) TTX, neuronal activity suppressed by injecting TTX (10 $\mu$M) in the MEA (10,100 FIDs, ≈17 min).

***Data processing.*** The first 100 FIDs per data set were discarded to ensure signal steady state. To minimize high frequency noise (>10 Hz), the remaining 10,000 FIDs were multiplied by (apodized) a cosine-bell function that reduced the weighting of the latter 512 points per FID. The phase and magnitude of the FID signal was calculated from the raw complex data, resulting in one magnitude and one phase data set (10,000 $FIDs_{mag|phase}$ × 1,024 per FID) for both the PRE and TTX states per MR session. MR phase and magnitude time series were computed with a single phase and magnitude value per repetition time as follows: the mean magnitude and phase FID were computed for each data set and were subtracted from each of the 10,000 FIDs in the data set. The resulting zero-mean FIDs were averaged per repetition time, yielding a 10,000-point MR time series of the net magnitude or phase change per repetition time. MR time series were then detrended and time points above the mean (=0) ± 4 × time series SD were discarded to correct for linear drift and/or scanner noise.

***MR/EEG data analysis.*** Spectra were computed for the average EEG, MR magnitude, and MR phase time series. The total signal power was computed for the frequency range 0–5 Hz, and differences in signal power between PRE and TTX states were calculated for both EEG and MR spectra. The amplitude-weighted mean frequency (spectral centroid) for the 0–5 Hz range was computed for the EEG and MR spectra to evaluate the distribution of frequencies. Linear regression was performed on the EEG and MR data for the PRE vs. TTX percent signal power decrease and spectral centroid to evaluate the relationship between EEG and MR. Spearman's rank correlation was performed between EEG and MR spectra after aligning the spectra based on their difference in spectral centroid. The correlation analysis also was performed on the EEG spectra for the two cultures with the additional 60-min recordings. Power spectra were calculated for the initial and final 17 min of the 60-min recordings and were compared with the PRE-state EEG spectra for the same cultures. Magnetic field changes corresponding to the observed MR signal changes were calculated as: $\Delta B = \Delta\varphi/(\gamma\tau 180/\pi)$ (tesla), where $\Delta\varphi$ is MR phase change between the PRE and TTX states, $\gamma$ is the proton gyromagnetic ratio ($2.68 \times 10^8 rad/(T\,\mathrm{sec})$), and $\tau$ is the time to the center of the FID signal readout (50 ms). For display, the spectra were normalized to the 0–5 Hz spectral power of the PRE state, for the EEG, MR phase, and MR magnitude individually, to allow for a direct comparison between the different measurements obtained for each culture.

**3-T Imaging.** ***Experiment setup.*** For the 3-T imaging experiment, the cultures were prepared on 24 × 12 mm glass coverslips with 0.2 mm thickness and cultivated according to the "roller tube" approach immersed in 0.8 ml of culture medium (19). For scanning, the coverslips were immersed in the center of a spherical glass container (10 cm diameter) filled with artificial cerebrospinal fluid that contained 126 mM NaCl, 0.3 mM $NaH_2PO_4$, 2.5 mM KCl, 0.3 mM $KH_2PO_4$, 1.6 mM $CaCl_2$, 1.0 mM $MgCl_2$, 0.4 mM $MgSO_4$, 26.2 mM $NaHCO_3$, and 11 mM D-glucose saturated with 95% $O_2$ and 5% $CO_2$ (Fig. 9, which is published as supporting information on the PNAS web site). This preparation was chosen to prevent image distortions caused by the air and culture medium interface in the MEA chamber. The sample was held in place with a hallow tube that also was used to administer fluids. The temperature was held at 36 ± 2°C by

using gel heating pads. The spherical container was secured in the RF receive coil with rubber constraints.

***Data acquisition.*** Four cultures were scanned by using a 3-T General Electric (Milwaukee, WI) VH/i MRI scanner (3 T/90 cm, whole body gradient inset 40 mT/m, slew rate 150 T/m per s) with RF transmit/receive volume and 10-inch RF receive-only surface coils (Nova Medical, Wilmington, MA) and a SE EPI (repetition time, 1 s; echo time, 60 ms; flip angle, 90°; field of view, 18 cm; imaging matrix, $64 \times 64$, resulting in a voxel volume of 24 $mm^3$; readout window, 44 ms, dwell time, 4 $\mu$s). In this study, a SE EPI sequence was chosen to minimize slow phase fluctuations because of hardware instabilities. The 180° "refocusing" pulse allows the spin-echo sequence to be selectively "tuned" to transient phase shifts (or magnitude changes) that take place within the time between the 90° excitation pulse and the 180° refocusing pulse or (identically) the time between the 180° refocusing pulse and the center of the readout window that takes place at the spin-echo. Any phase shifts that occur on a slower time scale become "refocused" by the 180° pulse.

Four 3-mm-thick slices were prescribed orthogonal to the coverslip. High-resolution structural fast spin-echo images were acquired before EPI for localization of the culture on the coverslip (image matrix, $256 \times 256$; field of view, 18 cm; slice thickness, 3 mm, 10 slices, coronal plane) (Fig. 9*b*). Six hundred SE EPI images were acquired per slice for the PRE state, followed by the TTX state (10 min per state).

***Data processing.*** The SE EPI data sets were reconstructed into magnitude and phase images. The first 10 images per data set were discarded to ensure signal steady state. The mean magnitude and phase image was computed for each data set and was subtracted from each voxel time course in the respective magnitude or phase data set. The resulting zero-mean time courses were detrended to correct for linear drift. The resulting data were depicting net magnitude and phase changes for the duration of the data acquisition. A sliding-window fast Fourier transform was used to calculate phase and magnitude spectra. The sliding-window fast Fourier transform enhances the power of periodic signals, such as neuronal activation signals, while minimizing the power of random signals, such as thermal noise (32). Phase and magnitude spectra were calculated per voxel with a sliding-window of 150 points (s) and a sliding step of 10 s (0.1 Hz) in the range of the burst activation frequencies observed in this type of culture.

***Data analysis.*** The culture location was identified from the structural images. For each voxel, differences in signal power at each spectral peak (peak area) between the PRE and TTX data sets were computed. Voxels near the surface of the container were excluded from the analysis to avoid edge artifacts. Spectral peaks were attributed to neuronal activity if and only if they exhibited reduced power in the TTX state for voxels corresponding to the culture location. The signal power difference for the selected peaks was averaged over the voxels corresponding to the culture location as a measure of the suppression of neuronal activity in the culture. Maps of MR signal power changes were computed as the per voxel power difference between the PRE and TTX state of the selected spectral peaks. Magnetic field changes corresponding to the observed SE EPI MR signal changes were calculated as $\Delta B = \Delta\varphi/(\gamma \cdot TE \cdot 180/\pi)$ (tesla), where $\Delta\varphi$ is MR phase change between the PRE and TTX states, and $TE$ is echo time (60 ms). For display, the spectra were normalized to the total spectral power of the PRE state, for MR phase and MR magnitude individually, to allow for a direct comparison between the two measurements.

We thank C. V. Stewart for preparation of cultures and technical assistance with electrical recordings and N. F. Ramsey (Rudolf Magnus Institute, Utrecht University, Utrecht, The Netherlands) for critical review of the manuscript.

1. Hamalainen M, Hari R, Ilmoniemi RJ, Knuutila J, Lounasmaa OV (1993) *Rev Mod Phys* 65:413–497.
2. Lewine JD, Orrison WW (1995) in *Functional Brain Imaging*, eds Orrison WW, Lewine JD, Sander JA, Hartshorne MF (Mosby, St. Louis), pp 327–368.
3. Romani GL (1989) in *Advances in Biomagnetics*, ed Wiliamson S (Plenum, New York).
4. George JS, Aine CJ, Mosher JC, Schmidt DM, Ranken DM, Schlitt HA, Wood CC, Lewine JD, Sanders JA, Belliveau JW (1995) *J Clin Neurophysiol* 12:406–431.
5. Moonen CTW, Bandettini PA (1999) *Functional MRI* (Springer, Heidelberg).
6. Lin F-H, Witzel T, Hamalainen M, Dale AM, Belliveau JW, Stufflebeam SM (2004) *NeuroImage* 23:582–595.
7. Bodurka J, Jesmanowicz A, Hyde JS, Xu H, Estkowski L, Li SJ (1999) *J Magn Reson* 137:265–271.
8. Bodurka J, Bandettini PA (2002) *Magn Reson Med* 47:1052–1058.
9. Song AW, Takahashi AM (2001) *Magn Reson Imaging* 19:763–767.
10. Truong T-K, Wilbur JL, Song AW (2006) *J Magn Reson* 179:85–91.
11. Konn D, Gowland P, Bowtell R (2003) *Magn Reson Med* 50:40–49.
12. Park TS, Lee SY, Park J-H, Lee SY (2004) *NeuroReport* 15:2783–2786.
13. Park TS, Lee SY, Park JH, Cho MH, Lee SY (2006) *Physiol Meas* 27:181–190.
14. Joy M, Scott G, Henkelman M (1989) *Magn Reson Imaging* 7:89–94.
15. Singh M (1994) *IEEE Trans Nucl Sci* 41:349–351.
16. Xiong J, Fox PT, Gao J-H (2003) *Hum Brain Mapp* 20:41–49.
17. Chu R, de Zwart JA, van Gelderen P, Fukunaga M, Kellman P, Holroyd T, Duyn JH (2004) *NeuroImage* 23:1059–1067.
18. Kamei HIK, Yshikawa K, Ueno S (1999) *IEEE Trans Magn* 35:4109–4111.
19. Konn D, Leach S, Gowland P, Bowtell R (2004) *Magn Reson Imaging* 22:1413–1427.
20. Plenz D, Kitai S (1998) *J Neurosci* 18:266–283.
21. Beggs J, Plenz D (2003) *J Neurosci* 23:11167–11177.
22. Bracewell RN (2000) in *The Fourier Transform and Its Applications* (McGraw–Hill, New York), 3rd Ed, p 577.
23. Xue Y, Gao J-H, Xionga J (2006) *NeuroImage* 31:550–559.
24. Trubel HKF, Sacolick LI, Hyder F (2006) *J Cereb Blood Flow Metab* 26:68–78.
25. Gorbach AM, Heiss J, Kufta C, Sato S, Fedio P, Kammerer WA, Solomon J, Oldfield EH (2003) *Ann Neurol* 54:297–309.
26. Marshall I, Karaszewski B, Wardlaw JM, Cvoro V, Wartolowska K, Armitage PA, Carpenter T, Bastin ME, Farrall A, Haga K (2006) *Magn Reson Imaging* 24:699–706.
27. Zhong J, Petroff OA, Prichard JW, Gore JC (1993) *Magn Reson Med* 30:241–246.
28. Darquié A, Poline J-B, Poupon C, Saint-Jalmes H, Le Bihan D (2001) *Proc Natl Acad Sci USA* 98:9391–9395.
29. Tasaki I, Nakaye T, Byrne PK (1985) *Brain Res* 331:363–365.
30. Dietzel I, Heinemann U, Hofmeier G, Lux HD (1980) *Exp Brain Res* 40:432–439.
31. Caeser M, Schuz A (1992) *J Hirnforsch* 33:429–443.
32. Proakis JG, Manolakis DG (1996) in *Digital Signal Processing: Principles, Algorithms, and Applications* (Prentice–Hall, Englewood Cliffs, NJ), pp 896–920.